Engineering Fracture Mechanics 286 (2023) 109292

Contents lists available at ScienceDirect

Engineering Fracture Mechanics

journal homepage: www.elsevier.com/locate/engfracmech

On the strain energy release rate and fatigue crack growth rate in metallic alloys

Emiel Amsterdam [a,*], Jan Willem E. Wiegman [a], Marco Nawijn [b], Jeff Th.M. De Hosson [c]

[a] Royal Netherlands Aerospace Centre (NLR), Marknesse, the Netherlands
[b] Colosso, Uffelte, the Netherlands
[c] Dept. Applied Physics, Zernike Institute for Advanced Materials, University of Groningen, Groningen, the Netherlands

ARTICLE INFO

Keywords:
Linear elastic fracture mechanics
Fatigue
Design
Engineering
Metals

ABSTRACT

The field of fracture mechanics started with Griffith's energy concept for brittle fracture in 1920. In 1963, Paris *et al.* used a fracture mechanics' parameter to introduce an equation for the fatigue crack growth rate in ductile materials and this equation is now commonly known as the 'Paris law'. However, the Paris law and the semi-empirical models that followed ever since do not fully account for the main intrinsic and extrinsic properties involved with fatigue crack growth in metallic alloys. In contrast, here a dimensionally correct fatigue crack growth rate equation is introduced that is based on the original crack driving force as introduced by Griffith and the presence of plasticity in a metal to withstand crack propagation. In particular it is shown that the fatigue crack growth rate shows a power law relationship with the cyclic strain energy release rate over the maximum stress intensity factor. The new description corrects for the ratio between the minimum and maximum stress in a cycle during constant amplitude loading and for crack growth retardation under variable amplitude loading. The method has been successfully applied to variable amplitude crack growth with spectra that are representative of different fatigue dominated aircraft locations. As such, it allows for accurate predictions of variable amplitude fatigue crack growth life in aerospace structures.

1. Introduction

The research field of fracture mechanics started with the introduction of Griffith's energy concept for brittle fracture in glass [1]. After establishing equivalency between an energy and a stress based approach, the propagation of a brittle crack was described by the concentration of elastic stress near the tip of the crack, the so-called stress intensity factor [2]. In 1963, Paris and Erdogan used the range of the stress intensity factor during a loading cycle to introduce an equation for the fatigue crack growth rate in ductile engineering materials [3]. This equation is now commonly known as the 'Paris law' [4]. However, the Paris law and the semi-empirical models that followed ever since do not fully account for the main intrinsic and extrinsic properties involved with fatigue crack growth in metallic alloys, e.g. the Young's modulus, plasticity and the applied stress range [4–8]. Fatigue crack growth depends on specific aircraft usage and the predictive capabilities of the current crack growth models for variable amplitude loading are inadequate due to the aforementioned limitations of the Paris law and other semi-empirical models [9–13]. This confines the aircraft operation to

* Corresponding author.
E-mail address: emiel.amsterdam@nlr.nl (E. Amsterdam).

https://doi.org/10.1016/j.engfracmech.2023.109292
Received 17 February 2023; Accepted 22 April 2023
Available online 27 April 2023

Nomenclature

a	Crack length
a_0	Crack length after zero cycles or turning points
a_f	Crack length after f turning points
a_r	Crack length at a specific fatigue crack growth rate
b	Burgers vector
C	Crack growth rate constant
d_i	Characteristic length scales
E	Young's modulus
f	Number of turning points
G	Strain energy release rate per unit thickness
G_C	Critical strain energy release rate per unit thickness
G_{max}	Maximum strain energy release rate per unit thickness
G_I	Strain energy release rate of a linear elastic, quasi-static crack in mode I
h	Power law exponent in the FSI
J_c	Critical value of the J-integral
J_{max}	J-integral at the maximum stress
J_{min}	J-integral at the minimum stress
K	Stress intensity factor
K_{max}	Maximum stress intensity factor
K_{mss}	Stress intensity factor for the MSS
K_{ref}	Stress intensity factor for the applied reference stress
N	Cycles
n, j, m	Power law exponents
p, q	Experimentally determined parameters
r_0	Atomic spacing
R	Stress ratio
R_t	Turning point stress ratio (with respect to the MSS)
S	Stress
S_{max}	Maximum stress
S_{min}	Minimum stress
S_{ref}	Applied reference stress during a FCGR test
ν	Poisson's ratio
V_r	Reference voltage
W	Specimen width
β	Geometry factor
ΔG	Cyclic strain energy release rate per unit thickness
ΔJ	Range of the J-integral
ΔK	Stress intensity factor range
ΔK_{eff}	Effective stress intensity factor range
ΔS	Stress range
$\Delta U'$	Cyclic strain energy density (CSED)
$\dot{\varepsilon}$	Strain rate
$\frac{K_{max}}{E}$	Maximum strain intensity factor
$\frac{da}{dN}$	Fatigue crack growth rate per cycle
$\frac{da}{dNA}$	Fatigue crack growth rate per variable amplitude cycle in spectrum A
$\frac{da}{dNB}$	Fatigue crack growth rate per variable amplitude cycle in spectrum B
$\frac{\Delta K}{E}$	Strain intensity factor range
$f(R)$	Stress ratio function
$\varphi(R)$	Crack closure correction function
AA	Aluminium alloy
CA	Constant amplitude
CSED	Cyclic strain energy density
DCPD	Direct current potential drop
EDM	Electric discharge machined
FCGR	Fatigue crack growth rate
FSI	Fatigue severity index
LEFM	Linear elastic fracture mechanics

LW	Wing lower skin
M(T)	Middle Tension
MSS	Maximum spectrum stress
PZR	Plastic zone radius
SSY	Small scale yielding
VA	Variable amplitude
WRBM	Wing root bending moments

the usage spectrum that was applied during the full scale fatigue test of the aircraft.

Here a dimensionally correct crack growth rate equation for tension–tension fatigue is introduced that accounts for the main intrinsic and extrinsic properties involved with fatigue crack growth in ductile materials. It will be shown that the new description intentionally corrects for the ratio between the minimum and maximum stress in a cycle during constant amplitude loading and for crack growth retardation under variable amplitude loading.

2. Theoretical background

Griffith used an energy concept to explain the difference between the theoretical strength of brittle materials and the experimentally observed strength [1]. Griffith's criterion states that unstable propagation of a quasi-stationary crack occurs upon loading when the energy released by a growing crack is greater than the energy needed to create new free surfaces. Combined with the work of Irwin [2], the unstable propagation of a quasi-stationary crack in brittle materials occurs when:

$$\frac{K_{max}^2}{E} = G_C \tag{1}$$

where K_{max} is the maximum stress intensity factor, which represents the stress field around the tip of the crack at the maximum applied stress, E is the Young's modulus and G_C is the critical strain energy release rate per unit thickness. The strain energy release rate per unit thickness, G, is generally considered as the driving force for crack propagation in brittle materials. Since only limited plastic deformation is expected in brittle materials, the stress field around the crack tip is largely linear elastic and hence this research field is called linear elastic fracture mechanics (LEFM).

Research in the late 1950′s indicated that the linear approximation of the stress field around the crack tip could also be used for small crack extension in ductile engineering materials during cyclic loading. The maximum strain energy release rate per unit thickness, G_{max}, and K_{max} were both used to correlate crack growth rates [5,14], but Paris *et al.* argued that the crack growth rate should also depend on R, i.e. the ratio between the minimum stress and the maximum stress in a constant amplitude cycle [14]. Subsequently, Paris and Erdogan showed in 1963 that fatigue crack growth rate (FCGR) data can be best correlated to the stress intensity factor range, ΔK, i.e. to the applied range of stress [3]:

$$\frac{da}{dN} = C((1-R)K_{max})^n \quad \text{(Paris law)} \tag{2}$$

where ΔK is written as a function of K_{max} and the stress ratio, R. Eq. (2) is frequently referred to as the Paris law [4]. The constant, C, and exponent, n, are material parameters that are determined experimentally and the values apply for the equation for which they are obtained. There is a linear relationship between log C and n, which indicates that the constant C is not independent of n and consequently the physical units of C depend on n [15]. The rationale for applying ΔK, i.e. K_{max} and the stress ratio R, is that identical intensity factors of the elastic stress field will result in identical yielding zones near the tips of the 'quasi-static' cracks in elastic–plastic material, provided that the zones where elastic–plastic yielding occurs are small compared to other geometric dimensions of the system, such as the crack length and thickness [14].

Frost and Greenan and, independently, Pearson showed for a stress ratio R of almost equal to zero that the crack growth rates for materials with different Young's moduli merge onto a single curve when the main factor governing the crack growth rate is the concentration of elastic strain at the crack tip [6,7], i.e.

$$\frac{da}{dN} = C\left(\frac{K_{max}}{E}\right)^n \tag{3}$$

However, Eq. (3) does not account for the stress range. Neither does it address the mean stress effect, which refers to the fact that the FCGR only correlates with ΔK at a given stress ratio. Basically, the term (1-R) in the Paris law is not sufficient to correlate all FCGR data to K_{max}. To solve the stress ratio problem, the range of an effective stress intensity factor, ΔK_{eff}, was introduced by Elber in 1971 to explain the different fatigue crack growth rates at different stress ratios for a given material [8]:

$$\frac{da}{dN} = C\left(\Delta K_{eff}\right)^n \tag{4}$$

where

$$\Delta K_{eff} = \varphi(R)\cdot(1-R)K_{max} \tag{5}$$

and

$$\varphi(R) = 0.5 + 0.4R \tag{6}$$

The introduction of the effective stress intensity factor range was argued from the observations that upon unloading after the maximum stress the crack faces already touch each other before the minimum stress is reached. Since a crack cannot propagate while it is closed, the stress range that can effectively be used for crack extension is shortened, hence the name effective stress intensity factor range. Different empirical functions for the crack closure correction functions, *$\varphi(R)$,* have been proposed [8,16]. It is noteworthy that the crack closure correction functions*,* being a rather simple multiplier to the original proposal of Paris and Erdogan, are all based on experiments and not on theoretical considerations.

Alternatively, to incorporate the influence of crack tip plasticity and to account for stress ratio effects, Walker included a K_{max} in the FCGR equation in 1970, just prior to the introduction of ΔK_{eff} by Elber [8,17]. Walker included K_{max} by an equivalent stress[1] resulting in a two parameter modified Paris-type FCGR equation [17]:

$$\frac{da}{dN} = C\Delta K^{j}K_{max}^{m} \tag{7}$$

Several modifications and justifications of Eq. (7) are discussed in literature where the material parameters j and m are either correlated or uncorrelated to each other [18–21]. The inclusion of K_{max} in the FCGR equation can be justified by a competition between brittle and ductile fatigue mechanisms, where the brittle mechanism is controlled by K_{max} and the ductile mechanism by ΔK, or by plasticity, where a change in K_{max} at a given ΔK would cause a change in the radius of the plastic zone. The latter is proportional to K_{max} squared, according to experimental- and theoretical work as well as finite element modelling [2,22–27]. During fatigue crack growth the plastic zone has to be displaced over a distance equal to the crack increment after each cycle. As a result, more energy is consumed by plastic deformation for a larger K_{max} at a given ΔK. However, Eq. (7) is also a Paris-type power law relationship that depends on K_{max} and a function of R:

$$\frac{da}{dN} = C\left((1-R)^{\frac{n-m}{n}}\cdot K_{max}\right)^{n} \tag{8}$$

where $n = j + m$. In fact, Eqs. (2), (4) and (8) are all power laws with exponent n and K_{max} times an additional function of R under the exponent:

$$\frac{da}{dN} = C(f(R)\cdot K_{max})^{n} \tag{9}$$

where the stress ratio function $f(R)$ is used to account for the stress range ΔS in a constant amplitude cycle, which is typically regarded as the driving force, and for the effect of stress ratio on the FCGR. Therefore, when the minimum stress changes *for a given maximum stress*, than both the stress range and the stress ratio change. However, in fact only one parameter changes, which is the minimum stress. *Thus, when the effect of the minimum stress in a constant amplitude cycle is properly incorporated in a theoretical framework, it should predict the FCGR for different minimum stresses and hence different stress ratios.*

Instead of using the stress range with the stress intensity factor Barsom used the cyclic strain energy release rate per unit thickness, ΔG, to correlate the FCGR of various metals in 1971 [28]:

$$\Delta G = \frac{(1-R^2)K_{max}^2}{E} \tag{10}$$

Barsom used ΔG to correlate the fatigue crack growth rates of steel, titanium and aluminium alloys, even though the experimental results showed better correlations for the *strain* intensity factor range [28,29]:

$$\frac{\Delta K}{E} = \frac{(1-R)K_{max}}{E} \tag{11}$$

The inverse proportional relationship of the Young's modulus with K_{max} was initially observed by Frost & Greenan and Pearson has been confirmed and discussed by others [4,6,7,30–37]. Note that Eq. (11) is different than Eq. (10), where the Young's modulus is inverse proportional with K_{max}^2.

It is notable that the cyclic strain energy release rate per unit thickness, ΔG, is widely used to correlate fatigue crack growth rates of composite materials, because G is easy to calculate and K is ill-defined in an inhomogeneous material even though they are correlated [38–40]. However, there is still an ongoing debate whether ΔG is the proper parameter of similitude for composite materials [40–42]. Chow *et al.* used ΔG to correlate the FCGR of various metals and polymers [43–45]. At a later stage, they included the critical strain energy release rate, G_c, and the G_{max} in the equation and represented it in a more generalized form to cover a wide range of materials [45,46]:

[1] In the paper the equivalent stress is called the effective stress. However, after the introduction of the crack closure by Elber in 1971, the effective stress range is nowadays associated with the difference between the maximum stress and the opening stress.

$$\frac{da}{dN} = C\frac{\Delta J^n}{J_c - J_{max}} \tag{12}$$

where J_c is the critical value of the J-integral and ΔJ the difference between the J-integral at the maximum stress (J_{max}) and minimum stress (J_{min}). There are others who also related the FCGR with ΔJ for short cracks, small scale yielding (SSY) and large scale yielding conditions, the latter being appropriate for region III in the fatigue crack growth curve or for low cycle fatigue [47–55]. Under SSY conditions the J-integral is equal to G and Eq. (12) can be expressed in terms of G.

3. Methods and materials

In this paper a phenomenological model is designed by examining the influence of the most important parameters and assessing their precise functionality in a fatigue crack growth rate (FCGR) equation. Many of the empirical models, like Eq. (2), are dimensionally incorrect and do not contain intrinsic material properties that are known to affect the FCGR, e.g. the Young's modulus [4,6,7]. Dimensional analysis has been performed in literature, but without conclusive results on the parameter of similitude for fatigue crack growth [12,34,56–59]. Characterisation of each parameter that influences the FCGR is the first step in a phenomenological model of fatigue crack growth. Constructing a dimensionally correct equation with those parameters is the second step.

As shown in the previous sections, it is common practice to use ΔK or K_{max} with a function of R as crack driving force for fatigue crack growth rate, where higher values of the crack driving force result in higher fatigue crack growth rates. Therefore, the applied maximum stress, the minimum stress and the crack length are the main parameters that affect the FCGR for a given material, geometry and environment and test frequency. The influence of the latter parameters are usually incorporated in the material constants, e.g. C and n of Eq. (2), and the geometry factor, β. During constant amplitude FCGR tests the only parameter that influences the FCGR during the test is the crack length. Since exact reconstruction of the a-N curve is possible for FCGR tests with a constant range of stress, the influence of the crack length on the FCGR has been fully characterised [60]. To characterise the influence of the remaining test parameters, a total of 61 middle tension (M(T)) specimens of 7075-T7351 were tested in constant amplitude tension–tension loading with a variety of minimum and maximum stresses, which resulted in 13 different stress ratios ranging from $R = 0.01$ to $R = 0.77$. Other test parameters were kept constant by only testing M(T) specimens, removed from plates with a single lot number, testing under lab air conditions and a single test frequency.

M(T) specimens with dimensions of 500 mm × 160 mm were obtained from aluminium alloy (AA) 7075-T7351 plate material with a thickness of 6.35 mm. Next to the 61 M(T) specimens of 7075-T7351, additional M(T) specimens from the same plates were given an annealing heat treatment at 415 °C for 2 hr, furnace cool to 230 °C at 30 °C/hr, 6 hr at 230 °C and air cool (treatment f from Table 13 in [61]) to investigate the effect of yield stress on the FCGR. The rolling direction was in the length of the M(T) specimens, hence loading-crack growth was in the L-T direction. Fatigue crack growth starter notches were central holes (1.6 mm diameter) with 0.7 mm deep electric discharge machined (EDM) slots on either side of the hole (total starter notch length of 3 mm). The EDM wire thickness was 0.16 mm. The area next to the starter notch was polished for optical crack growth measurements on both the front and rear side of the specimens.

Constant amplitude (CA) fatigue crack growth tests were performed using a 13.5 Hz sinusoidal load that was introduced in lab air environment by a servo-hydraulic test machine with a 200 kN load cell. The same maximum stress and stress ratio as for the actual test was used for pre-cracking the M(T) specimen to a single side crack length, a, of about 2 mm. The actual crack length after pre-cracking was measured with an optical travelling microscope.

Holes were present at 8 mm above and below the starter notch hole for copper pins. These were used for automated crack length measurements by direct current potential drop (DCPD). The current was introduced to the specimen at the clamps. The DCPD data was converted to crack length data using Equation A2.5 in ASTM E647 [62]. The reference voltage, V_r, in Equation A2.5 in ASTM E647 was adjusted for each specimen such that the crack length from the DCPD measurement at the start of the test was equal to the crack length measured with the optical travelling microscope after pre-cracking.

The stress intensity factor, K, for the M(T) specimens is calculated by:

$$K = \beta(a)S\sqrt{\pi a} \tag{13}$$

where S is the remotely applied stress, a the crack length and β the Feddersen final width correction that is calculated according to ASTM E647 [62]:

$$\beta = \sqrt{\sec\left(\frac{\pi a}{W}\right)} \tag{14}$$

where W is the width of the specimen.

Variable amplitude (VA) fatigue crack growth rate tests were performed on 7075-T7351 M(T) specimens from the same plates. The crack length vs. cycles (N) curves for constant and variable amplitude loading were fitted using the method described in Amsterdam *et al.* to obtain the FCGR per CA or VA cycle as a function of the crack length [60,63].

The number of VA cycles in the wing lower skin spectrum is 5563, where the number of VA cycles is half the number of turning points in a spectrum. The spectrum that is based on wing root bending moments (WRBM) of a fighter aircraft was modified three times to increase the severity of the spectra by randomly changing the stress for a large number of turning points (but keeping them between 0 MPa and the maximum spectrum stress). The WRBM spectrum and the three modifications have 1739 VA cycles. The WRBM spectra were applied with a reference stress of 90 MPa and the number of repeats during the FCGR tests ranged from 207 for the modified spectrum with the highest severity to 731 for the original WRBM spectrum. The wing lower skin spectrum was applied with a reference stress of 115 MPa and was repeated for at least 716 times during the FCGR tests. Three specimens were tested for each VA spectrum with an average frequency between 14 and 20 Hz for the severest WRBM-M3 and least severe wing lower skin spectra, respectively.

4. Results

4.1. Constant amplitude fatigue

Barsom used the range of the original crack driving force, ΔG, to correlate the fatigue crack growth rates of steel, titanium and aluminium alloys, even though the experimental results of Barsom and others show better correlations for the *strain* intensity factor range, $\Delta K/E$ [4,6,7,28,30–37]. However, the maximum *strain* intensity factor in Eq. (3) can easily be rewritten as a function of the maximum strain energy release rate by multiplying both the numerator and denominator by K_{max}:

$$\frac{da}{dN} = C\left(\frac{K_{max}}{K_{max}}\frac{K_{max}}{E}\right)^{n} \tag{15}$$

Combining Eqs. (15) and (10) so as to account for different stress ratios results in:

$$\frac{da}{dN} = C\left(\frac{\Delta G}{K_{max}}\right)^{n} = C\left(\frac{(1-R^{2})K_{max}}{E}\right)^{n} \text{for R} \geq 0 \tag{16}$$

where $\Delta G/K_{max}$ is the new parameter of similitude and ΔG can be regarded as the fatigue crack driving force and the inverse of K_{max} can be related to the presence of plasticity.

Fig. 1 shows a fatigue crack growth rate master curve for AA7075-T7351 [60]. By definition the FCGR curves for different stress ratios create a master curve when the correct parameter of similitude is used. If $\Delta G/K_{max}$ is the correct parameter of similitude for the fatigue crack growth rate, than $\Delta G/K_{max}$ should be constant for a specific fatigue crack growth rate, i.e.:

$$\Delta U^{'} \cdot \frac{2}{S_{max}} \cdot \beta\sqrt{\pi a} = constant \tag{17}$$

where $\Delta G/K_{max}$ is written as a function of cyclic strain energy density, ΔU':

$$\Delta U^{'} = \frac{(1-R^{2})S_{max}^{2}}{2E} \tag{18}$$

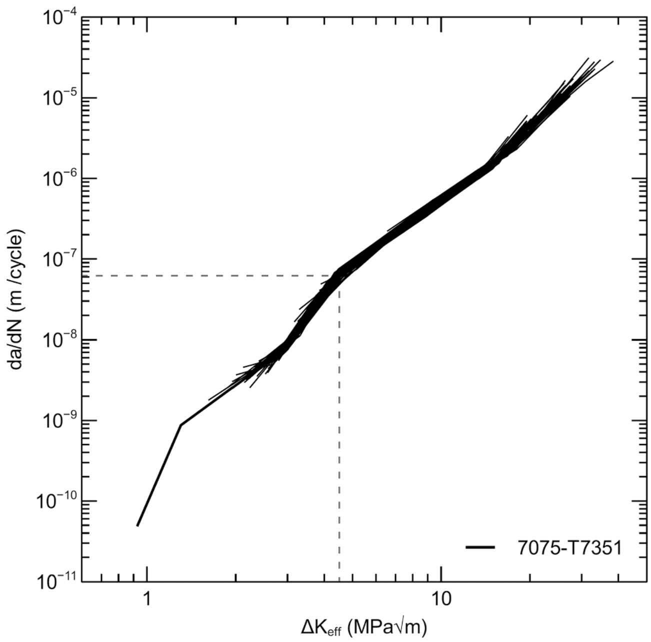

Fig. 1. Fatigue crack growth rate master curve as a function of ΔK_{eff} [60]. For this master curve ΔK_{eff} is used as the parameter of similitude, which is calculated using the Schijve crack closure correction: $\varphi(R) = 0.55 + 0.33R + 0.12R^2$ [34,35]. 54 specimens with 11 different maximum stresses and 13 different stress ratios are included in the master curve. The dashed lines indicate that the parameter of similitude is constant for the given da/dN.

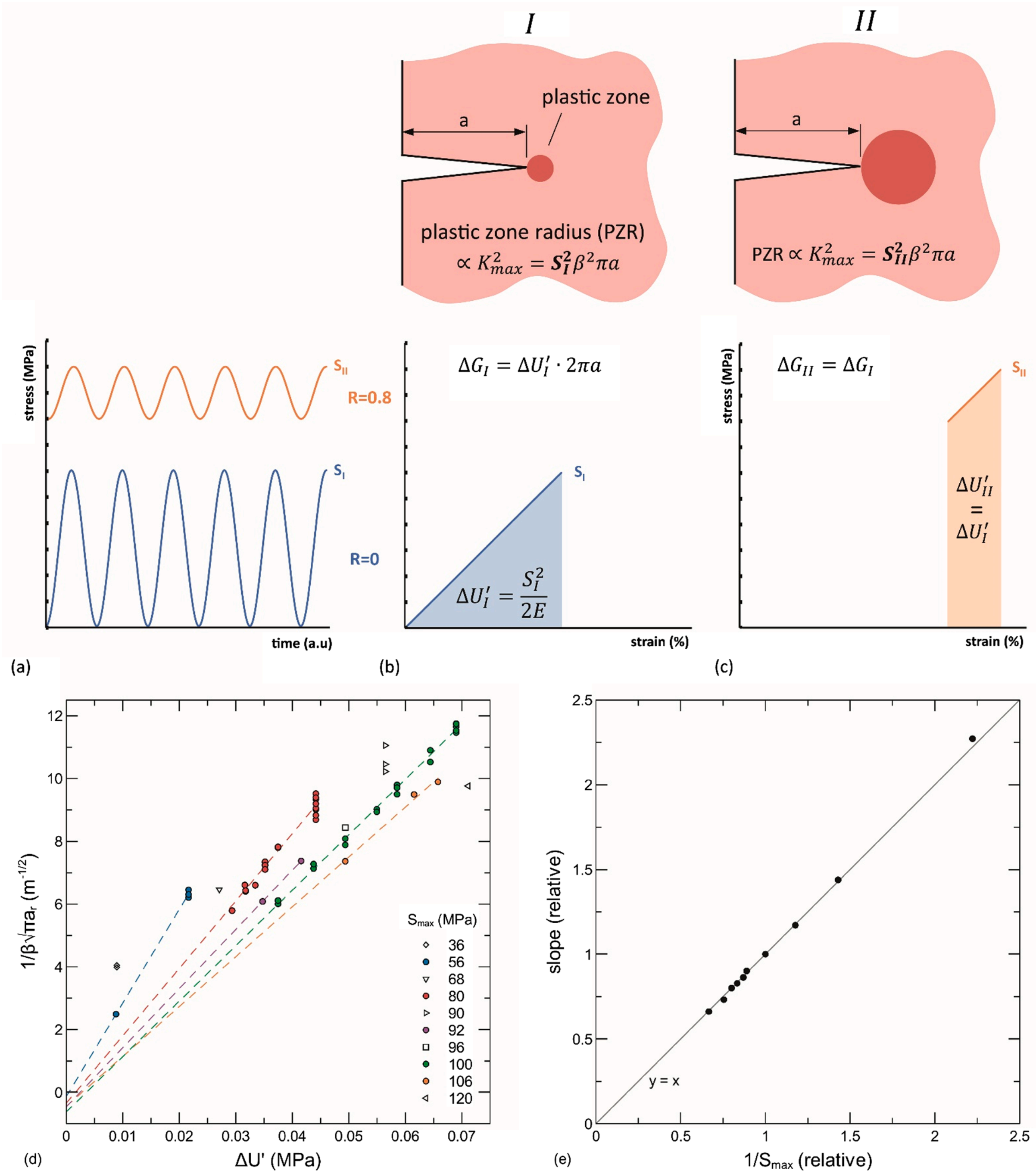

Fig. 2. (a) Schematic of cyclic loading tests as a function of time for two different stress ratios, but equal cyclic strain energy density, $\Delta U'$. (b) Schematic of stress–strain response and plastic zone radius for test I with $R = 0$. (c) Schematic of stress–strain response and plastic zone radius for test II with $R = 0.8$. The cyclic strain energy release rate, ΔG, is equal for both tests (d) Inverse crack length term at $6.18{\cdot}10^{-8}$ m/cycle as a function of the cyclic strain energy density for different S_{max}. The open data points correspond to specimens tested at only one stress ratio and the filled data points correspond to specimens tested at multiple stress ratios. The dashed lines are linear fits of the corresponding data. (e) relative slope as a function of the relative inverse S_{max}. The slope and maximum stress of the 80 MPa fit was used as a reference (see also Table 1).

Any change in the maximum and/or minimum stress should result in a change in crack length at which that specific FCGR occurs:

$$\frac{1}{\beta(a)\sqrt{\pi a}} = \frac{constant}{S_{max}} \cdot \Delta U' \tag{19}$$

Eq. (19) indicates that if $\Delta G/K_{max}$ is the correct parameter of similitude the inverse square root of the crack length at a given FCGR and S_{max} should be proportional to the cyclic strain energy density. For a given S_{max}, the cyclic strain energy density, ΔU', can be varied by varying the minimum stress (see Eq. (18)).

Fig. 2d shows that the inverse square root of the crack length at an FCGR of 6.18·10^{-8} m/cycle has a linear relationship with ΔU' *for a given maximum stress*. This FCGR lies in the middle of the FCGR curve and corresponds to a transition point with a large difference in the slope before and after the transition (see Fig. 1) [60]. Since each curve in Fig. 2d has a different intercept of the ordinate and a different number of data points, the slope of each curve for a particular maximum stress was determined using the intercept of $S_{max} =$ 80 MPa (see Table 1). Fig. 2e shows the relative slope of each maximum stress for the intercept of $S_{max} = 80$ MPa as a function of the relative inverse maximum stress. The slope and maximum stress of the 80 MPa fit was used as a reference. Fig. 2e clearly shows that the slope has an inverse relationship with the maximum stress (see Eq. (19)).

The linearity in both Fig. 2d and 2e is evidence that the parameter of similitude consists of two separate parameters, i.e. ΔG and K_{max}. In this work ΔG is related to the amount of energy that is available for crack extension and K_{max} is related to the amount of plastic energy absorbed during crack extension. It accounts for the increase of the plastic zone radius with increasing maximum stress intensity factor, which is not included in LEFM. When the same amount of cyclic strain energy is supplied to a specimen, the FCGR decreases with increasing maximum stress, because more energy is necessary to displace the larger plastic zone that results from a greater maximum stress (see Fig. 2). Eq. (16) does not violate the SSY criteria, because it still assumes that the cyclic strain energy release rate and that the influence of the plastic zone size are governed by the magnitude of the elastic stress field, hence by the stress intensity factor.

Whether physical closing of a fatigue crack upon unloading is responsible for the stress ratio effect has been the subject of debate since its introduction [13,64,65]. James concluded that despite numerous papers on the subject have been written, there is still considerable disagreement and confusion as to the nature, magnitude, measurement and interpretation of fatigue crack closure [13]. Especially, since the crack closure correction, $\varphi(R)$, is also applied for minimum stresses above the stress for which crack closure occurs ($R > 0.15$–0.35). Fig. 3 shows the comparison between the stress ratio functions $f(R)$ in Eq. (5), where $f(R) = \varphi(R)(1-R)$, for different crack closure corrections $\varphi(R)$ and the cyclic strain energy density (CSED) correction in Eq. (16); $1\text{-}R^2$. Since the crack closure corrections of Elber and Schijve are showing that $\Delta K_{eff} \approx \Delta K/2$ for $R = 0$, a factor ½ is incorporated in the CSED correction for the sake of comparison [8,16]. Fig. 3 shows that the stress ratio functions $f(R)$ are almost equivalent to the term $(1-R^2)\cdot 1/2$. This indicates that the empirically determined crack closure correction, $\varphi(R)$, was necessary to correct for the fact that the stress range was used in the FCGR equation instead of the cyclic strain energy density (CSED). This does not negate the physical opening and closing of the crack during loading and unloading, respectively, or the resulting bi-linearity of the stress–strain curve. It only indicates the crack closure phenomenon is not responsible for the observed stress ratio / mean stress effect.

Although Eq. (16) is a big step forward, it is still incorrect as far as physical units are concerned and does not contain pivot points as introduced earlier [60]. Many authors indicate that fatigue crack growth is governed by different micro-mechanisms and result in different fatigue crack growth rates, i.e. different slopes in the FCGR curve [19,66–78]. The change in micro-mechanism is usually reflected by a change in the fracture surface topography [19,67–71,74–78]. The transition from one micro-mechanism to the next occurs when the monotonic or cyclic plane strain plastic zone dimensions become equal to characteristic microstructural dimensions [66–69,72,73,76]. Amsterdam *et al.* introduced mathematical pivot points to accommodate for the changes in the FCGR slope and to make the argument of the power law dimensionless [60]. The parameter of similitude is $\Delta G/K_{max}$ and it has the physical unit of $\sqrt{\text{m}}$. Therefore, characteristic length scales, d_i, are introduced at which the micro-mechanisms of crack growth changes when the monotonic or cyclic plane strain plastic zone dimensions become equal to the characteristic microstructural dimensions [60,66–69,72,73,76]:

$$\frac{da}{dN} = \frac{da}{dN_i}\left(\frac{\Delta G}{K_{max}\sqrt{\pi d_i}}\right)^{n_i} \text{for R} \geq 0 \tag{20}$$

Table 1
Coefficients of linear regression in Fig. 2.

S_{max} (MPa)	Slope	Intercept	Slope	Intercept*
36			487.5	−0.345
56	298.3	−0.136	308.7	−0.345
68			251.3	−0.345
80	214.7	−0.345	214.7	−0.345
90			193.4	−0.345
92	188.4	−0.463	185.4	−0.345
96			177.8	−0.345
100	176.6	−0.625	171.8	−0.345
106	158.8	−0.444	157.2	−0.345
120			142.1	−0.345

* The intercept of the ordinate was fixed at the value for $S_{max} = 80$ MPa.

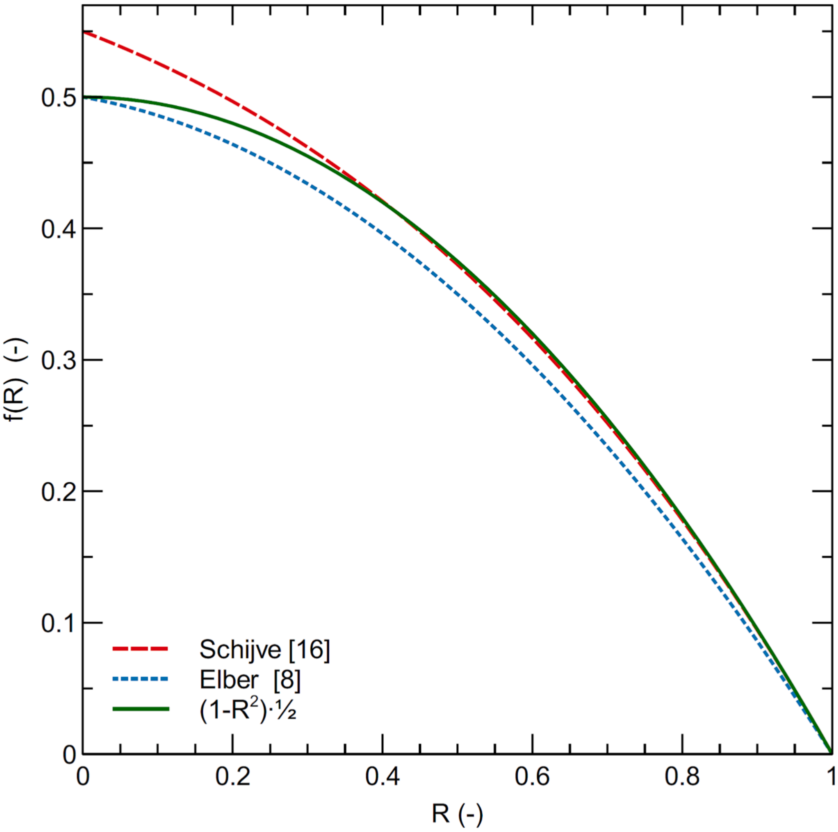

Fig. 3. Stress ratio functions for different crack closure corrections and the present model that is based on cyclic strain energy density (CSED). The CSED correction *(1-R^2)* was multiplied by 1/2 for the sake of comparison.

The term $\sqrt{\pi d_i}$ is related to the pivot points and holds the same physical unit as $\Delta G/K_{max}$. As a result, the argument of the power law is dimensionless and Eq. (20) becomes a dimensionally correct FCGR equation. The Young's modulus is included in Eq. (20) through ΔG and the resulting $E\sqrt{\pi d_i}$ term in Eq. (20) is similar to in literature proposed terms $E\sqrt{b}$ and $E\sqrt{r_0}$, where b is the magnitude of the Burgers.

vector and r_0 the atomic spacing [12,31,33,34,79,80]. Incorporating the terms $E\sqrt{b}$ and $E\sqrt{r_0}$ into the Paris law had the purpose of incorporating the Young's modulus dependency and correctness of the physical units. However, they were not introduced based on physical arguments as is the case for Eq. (20), where the Young's modulus dependency originates from the cyclic strain energy release rate, i.e. a fracture mechanics parameter, and the $\sqrt{\pi d_i}$ term originates from the presence of transition points in the FCGR curve that occur when the monotonic or cyclic plane strain plastic zone dimensions become equal to characteristic length scales in the microstructure [60]. Although the power law formulation is scale invariant and at this point the physical meaning of the internal length scales is unclear, the constant π is incorporated in the $\sqrt{\pi d_i}$ term to cancel out the constant $\sqrt{\pi}$ in the stress intensity factor that is raised to different exponents, n_i, without the presence of π in $\sqrt{\pi d_i}$. The transition from region I to region II of the FCGR curve occurs at about $7{\cdot}10^{-10}$ m/cycle and for small cracks this occurs at $\Delta G/K_{max} = 2.16{\cdot}10^{-5}$ m$^{1/2}$ [60]. This results in a d_i of $1.49{\cdot}10^{-10}$ m, which is close to the atomic radius of $1.43{\cdot}10^{-10}$ m for aluminium [81], and is in accordance with similar observations of Fleck *et al.* for the different metals [80]. Hence, the characteristic length scale for the first pivot point in the FCGR curve could be the atomic radius.

The definition of the strain energy release rate of a linear elastic, quasi-static crack in mode I, G_I, is different for plane strain and plane stress conditions [4]:

$$G_I = \begin{cases} G_I = \left(1 - \nu^2\right)\dfrac{K_I^2}{E}, & \text{for plane strain} \\[2ex] G_I = \dfrac{K_I^2}{E}, & \text{for plain stress} \end{cases} \tag{21}$$

where ν is Poisson's ratio. Although it is straightforward to calculate ΔG for a growing crack in a ductile material using $G_{I,\max}$ at the maximum stress and $G_{I,\min}$ at the minimum stress during a constant amplitude cycle, the physical meaning of ΔG is less clear. It becomes even more unclear at the transition from plane strain to plane stress, where the shear lips gradually develop [15,82,83]. Amsterdam *et al.* modelled the transition from plane strain and plane stress conditions using a pivot point and a different slope after the transition from plane strain to plane stress [15,60]. Therefore, Poisson's ratio is not included in Eq. (20), but the change in stress state is incorporated using different exponents, n_i, for plane strain and plane stress conditions (see also the following paragraphs related to Fig. 5) [60].

Although the yield stress has an effect on the plastic zone radius, it does not have a significant effect on the fatigue crack growth rate [34,36,84]. Amsterdam *et al.* already showed for a maximum stress of 80 MPa and $R = 0.1$ that the FCGRs of 7075-O (annealed) and 7075-T7351 are similar despite a factor 4 difference in yield stress [60]. In the same work it was shown that the FCGR increases with S_{max} at a given ΔK and R [60]. This effect is already present for S_{max} less than half the yield stress, but it increase considerably when the S_{max} approaches the yield stress. The phenomenon is referred to as 'the maximum stress-yield stress ratio phenomenon' [60]. Fig. 4 shows the FCGR of a 7075-T7351 and a 7075-O specimen. The maximum stress is well below half the yield stress of 433 and 108 MPa for 7075-T7351 and 7075-O, respectively [60]. Even though the FCGR is slightly higher at the beginning of the curve for 7075-T7351, the overall FCGR is similar for both alloys despite the factor 4 difference in yield stress. Although the yield stress has an effect on the plastic zone radius [27], it does not have an effect on the FCGR. Based on these experimental results the yield stress is not directly incorporated in Eq. (20) and dimensional analysis also indicates that it does not have to be included in the parameter of similitude or the argument of the power law. However, the yield stress does have an effect on the FCGR through the maximum stress-yield stress ratio phenomenon and how this effect can be incorporated in Eq. (20) will be discussed in the subsequent section. The yield stress becomes important for fatigue, where the initial crack lengths are very small and the maximum stress approaches the yield stress. Hence, for maximum stress less than half the yield stress the yield stress does not have an influence on fatigue crack growth rate or different mechanisms cancel each other out, but for fatigue, where the maximum stress approaches the yield stress, the yield stress is important and explains the influence of yield stress on the fatigue life.

The principal finding of this study is Eq. (20), where $\Delta G/K_{max}$ is the parameter of similitude that has been established based on the linearity in both Fig. 2d and 2e. However, the fact remains that the linear fits in Fig. 2d do not go through the origin. To elaborate on this further, Fig. 5 shows the FCGR as a function of $\Delta G/K_{max}$ for a maximum stress of 80 MPa and two different stress ratios. Only these stress ratios are shown for comparison, even though six different stress ratios were tested at $S_{max} = 80$ MPa. The transitions in the FCGR curves occur at specific $\Delta G/K_{max}$ values, which is as expected, but there are differences in the slopes of regions IIc (n_4) and IId (n_5) for the two different stress ratios [60]. The transition from region IIc to IId corresponds to the transition from plane strain to plane stress condition [60]. The insert shows that over a broader range of stress ratios the exponent n_4 decreases with increasing stress ratio and for exponent n_5 the opposite trend can be observed. If the exponents n_i of a power law curve with multiple pivot points are not the same, the curves cannot collapse onto a master curve by simply applying a correct parameter of similitude.

When the FCGR curves for $R = 0.1$ and $R = 0.54$ are inspected more closely, it is clear that the differences between these curves are

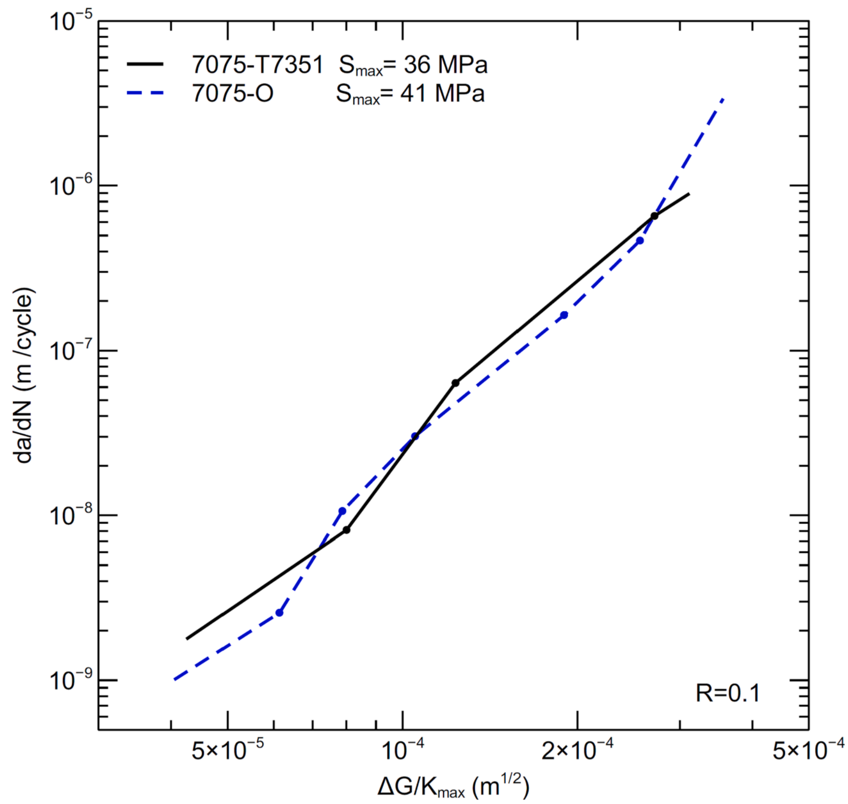

Fig. 4. FCGR as a function of $\Delta G/K_{max}$ for a 7075-T7351 and a 7075-O (annealed) specimen.

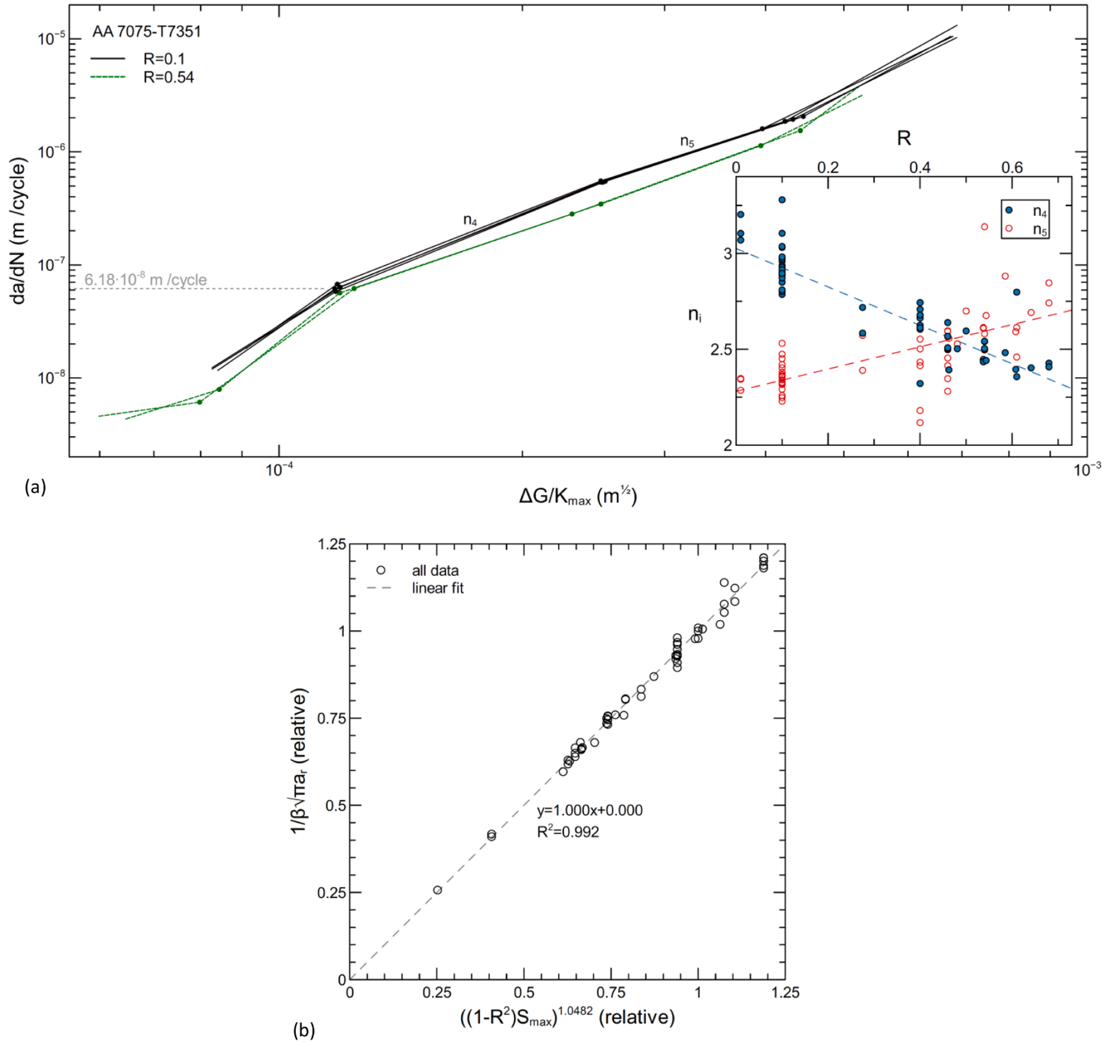

Fig. 5. (a) FCGR as a function of $\Delta G/K_{max}$ for four specimens tested at $R = 0.1$ and two specimens tested at $R = 0.54$. $S_{max} = 80$ MPa for all six specimens. The insert shows the exponent of regions IIc (n_4) and IId (n_5) as a function of the stress ratio for all specimens. The dashed lines are linear fits of the corresponding data. (b) Relative inverse crack length term at $6.18{\cdot}10^{-8}$ m/cycle as a function of the relative stress term for all specimens. One specimen with $S_{max} = 100$ MPa and $R = 0.4$ was used as reference specimen. The dashed line shows the linear fit.

not limited to differences in the exponents n_4 and n_5. Also the FCGR of the second pivot point in the $R = 0.54$ curve is slightly lower compared to the first one of the $R = 0.1$ curve. The figure shows that on average the FCGR over a range of $\Delta G/K_{max}$ has decreased for a higher stress ratio. It is possible that crack growth process is slightly less efficient at higher stress ratios due to interactions between the monotonic and cyclic plastic zone or less re-sharpening of the crack tip [4]. This introduces a new stress ratio dependency and an additional correction is necessary to put the $R = 0.1$ and $R = 0.54$ curves with the same S_{max} on top of each other *at* $6.18{\cdot}10^{-8}$ *m/cycle*. The additional stress ratio dependency as well as the aforementioned maximum stress-yield stress ratio phenomenon can be taken into account as follows:

$$\frac{da}{dN} = \frac{da}{dN_i}\left(\left(1 - R^2\right)^q \frac{S_{max}^p}{E}\frac{\beta\sqrt{\pi a}}{\sqrt{\pi d_i}}\right)^{n_i} \text{for R} \geq 0 \tag{22}$$

where q and p are experimentally determined parameters that account for additional small influences of R and S_{max} on the FCGR, respectively.

Fig. 5b is a contraction of Fig. 2d and 2e and shows that the inverse crack length term at $6.18{\cdot}10^{-8}$ m/cycle is proportional to the normalized stress related term in Eq. (22) when parameters q and p are both 1.0482. For these values the proportionality constant and intercept are unity and zero within four digits, respectively. Hence, the remaining differences between all FCGR curves at $6.18{\cdot}10^{-8}$ m/cycle are corrected for by the *additional* factors $(S_{max})^{0.0482}$ and $(1\text{-}R^2)^{0.0482}$.

Note that the introduction of the parameters q and p is one method to quantify the remaining differences in the FCGR curve at

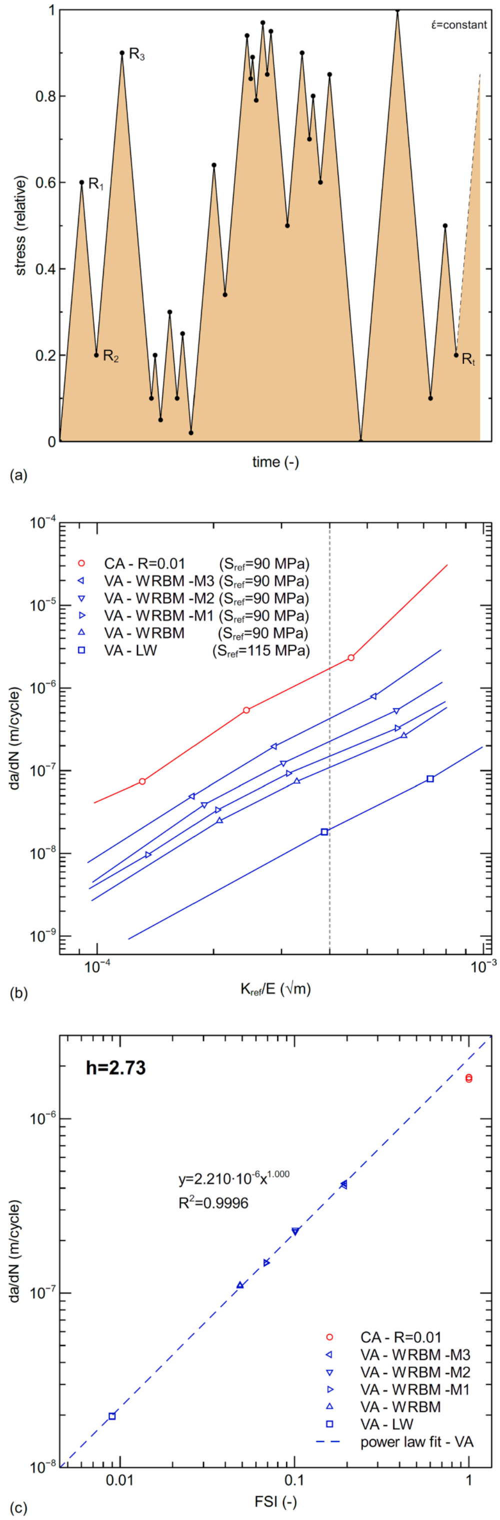

Fig. 6. (a) Schematic of a normalized variable amplitude spectrum as a function of time. The spectrum is plotted with a constant strain rate, $\dot{\varepsilon}$. (b) Average fatigue crack growth rate *per cycle* as a function of K_{ref}/E for five VA spectra and constant amplitude loading with $R = 0.01$. Each curve corresponds to a specimen and only one specimen per spectrum is shown for clarity. (c) FCGR at $K_{ref}/E = 4{\cdot}10^{-4}\ \sqrt{\mathrm{m}}$ as a function of FSI for three specimens per VA spectra and per CA loading with $R = 0.01$ (see also grey dotted line in (b)). The FSI was determined with $h = 2.73$.

$6.18{\cdot}10^{-8}$ m/cycle and for this range of S_{max}. As such, the main purpose of Eq. (22) and Fig. 5 is to show that the additional stress ratio dependency as shown in Fig. 5 and the maximum stress-yield stress ratio phenomenon as introduced in Ref. [60] are the reasons why the fits in Fig. 2d do not go through the origin. Addressing these observations and their physical mechanism is the subject of future work. Eq. (20) is the newly proposed equation and the equation only contains the pivot points as fitting parameters for a given material and environment. The pivot points are basically equal to the numbers in tabular FCGR data [85]. The exponents n_i are determined by the pivot points. Hence the number of fitting parameters in Eq. (20) are the same as in the Paris law for a linear FCGR curve in region II, i.e. da/dN_1 and n_1 if the atomic radius is used for d_1, and increases for a multi-linear FCGR with increasing number of pivot points.

4.2. Variable amplitude fatigue

In general most engineering structures and components are subjected to cyclic loading with variable amplitude. Small amplitude cycles that follow after a larger amplitude cycle lead to less crack growth compared to the same small amplitude cycles prior to the larger amplitude cycle. Although Eq. (20) has been derived for constant amplitude fatigue crack growth, here an important finding is that it can also be used for a variable amplitude model that accounts for crack growth retardation. During variable amplitude loading the crack growth is retarded after the occurrence of a large stress peak in the spectrum. Since the K_{max}^{-1} term in Eq. (20) is related to the plastic zone radius of the maximum stress in a loading cycle, crack growth retardation can be accounted for by using the maximum stress of a large stress peak for the K_{max}^{-1} term of the smaller amplitude cycles that follow afterwards. In essence, this indicates that crack growth from the smaller amplitude cycles occurs in the plastic zone created by the large stress peak earlier in the spectrum. The latter assumption is similar to the older Wheeler retardation model [86].

Each variable amplitude spectrum can be normalized by the maximum stress in the spectrum, i.e. the maximum spectrum stress (MSS), and R_t becomes the ratio between the stress at a turning point t and the MSS. For the boundary condition that the variable amplitude spectrum and the maximum spectrum stress is repeated before the crack grows out of the plastic zone of the MSS, the crack growth rate for a half cycle, i.e. between two turning points t and t-1, can be written as:

$$\frac{da}{dt} = \frac{da}{dt}_i \left(\frac{\left|R_t^2 - R_{t-1}^2\right| K_{MSS}^2}{K_{MSS} E \sqrt{\pi d_i}} \right)^{n_i} \text{for } \mathrm{R_t} \geq 0 \tag{23}$$

where K_{MSS} is the stress intensity factor for the MSS. Eq. (23) is rewritten as:

$$\frac{da}{dt} = \left|R_t^2 - R_{t-1}^2\right|^{n_i} \cdot \frac{da}{dt}_i \left(\frac{K_{MSS}}{E\sqrt{\pi d_i}} \right)^{n_i} \text{for } \mathrm{R_t} \geq 0 \tag{24}$$

Here the absolute value implies that the unloading part of a VA cycle contributes equally to crack growth as the loading part of a VA cycle. The crack length for a total of f turning points after the MSS, a_f, is:

$$a_f = a_0 + \sum_{t=1}^{f} \left|{R_t}^2 - {R_{t-1}}^2\right|^{n_i} \cdot \frac{da}{dt}_i \left(\frac{K_{MSS,t}}{E\sqrt{\pi d_i}} \right)^{n_i} \text{for } \mathrm{R_t} \geq 0 \tag{25}$$

where a_0 is the crack length after the MSS. $K_{MSS,t}$ is the stress intensity factor during the t^{th} turning point and is a function of the crack length prior to the t^{th} turning point, a_{t-1}. For a *given normalized spectrum* and limited crack growth after a spectrum block, R_t is independent of the crack length and the applied reference stress, S_{ref}, during the FCGR test. Hence, the term with R_t can be summed separately from the term with the stress intensity factor. The summation of the turning point ratios in a spectrum can be divided by the total number of turning points to provide an average fatigue severity index (FSI):

$$FSI = \frac{1}{f} \sum_{t=1}^{f} \left|{R_t}^2 - {R_{t-1}}^2\right|^{h} \text{for } \mathrm{R_t} \geq 0 \tag{26}$$

where n_i in Eq. (25) is replaced by a single value, h. The FSI of a spectrum is proportional to the average of the strain energy between turning points to the power h and Fig. 6 illustrates that the FSI is therefore related to the area under the spectrum when plotted with a constant strain rate. Hence, the FSI is related to the average energy in a spectrum that is available for crack growth and can act as the crack driving force, similarly as ΔG in Eq. (20) for constant amplitude loading. The approach is similar to the block approach, where the average crack growth per spectrum block is used [87,88]. For constant amplitude loading with $R = 0$ the FSI is equal to unity and independent of the exponent h.

Fig. 6 shows the *average* fatigue crack growth rate *per VA cycle* as a function of K_{ref}/E for five VA spectra with $0 \leq R_t \leq 1$ and for constant amplitude loading with $R = 0.01$. K_{ref} is stress intensity factor for the applied reference stress, S_{ref}, during a FCGR test using a normalized spectrum and hence equal to K_{MSS} of the unnormalized stress spectrum. The five spectra include a spectrum that is based on the VA loading of the wing lower skin of a commercial airliner, a spectrum that is based on wing root bending moments (WRBM) of a fighter aircraft and three modifications to the WRBM spectrum that increased the severity. The five spectra differ in severity, which result in predominately vertical translation of the FCGR curve, but the shapes of the FCGR curves are similar. Three specimens were tested for each VA spectra and for constant amplitude loading with $R = 0.01$. However, only one curve per specimen is shown in Fig. 6b for clarity. The vertical translation between VA FCGR curves is also accompanied by a small horizontal shift. The FSI can be determined for each spectrum, where the exponent h is the single parameter. Fig. 6c shows that for $h = 2.73$ there is a proportional relationship between the average fatigue crack growth rate per VA cycle at $K_{ref}/E = 4{\cdot}10^{-4}\ \sqrt{m}$ and the FSI. The results of the three specimens per VA spectra are similar, such that the data points in Fig. 6c are on top of each other. The parameter h in Eq. (26) can be regarded as an average of the exponents n_i. When the *a-N* curves of the specimens tested with a maximum stress between 80 and 100 MPa and a stress ratio between 0 and 0.5 are fitted with a single exponent, than the average and standard deviation of the exponent for these specimens is 2.75 ± 0.06. Since the *a-N* curves are fitted directly with a single exponent, instead of fitting the multi-linear FCGR curve with a single slope in the da/dN vs $\Delta G/K_{max}$ domain, the single exponent corresponds to the *weighted* average of the slope of the constant amplitude FCGR curve. The higher slope in region III of the FCGR curve has limited influence on the single exponent, because there are limited cycles in that part of the a-N curve and the fatigue crack growth life does not change much with a change in the region III slope. The *a-N* curves of the other specimens with a lower maximum stress or a higher stress ratio can also be described well with an exponent of 2.75, but with a lower power law constant.

Since the proportional relationship in Fig. 6c does not go through the CA data and a small horizontal shift in the FCGR curve with decreasing FSI can be observed in Fig. 6b, it is preferred to determine the FCGR curve of spectrum B relative to a known FCGR curve of spectrum A with a similar FSI:

$$\frac{da}{dN_B} = \frac{FSI_B}{FSI_A}\cdot\frac{da}{dN_{A,i}}\left(\frac{K_{ref}}{E\sqrt{\pi d_{A,i}}}\right)^{n_{A,i}} \tag{27}$$

The main advantage of the FSI is that the actual spectrum can be used and cycle counting methods, such as the rain-flow cycle counting method [89,90], are unnecessary. The FSI is a simple summation with an exponent h that is equal to the *weighted* average slope of the constant amplitude FCGR curve and can be used for different types of VA spectra and different severities.

The novel method has been applied for an international challenge to blindly predict the VA crack growth in 7075-T7351 material, where the specimen geometry and spectrum are representative of the lower surface of a large transport aircraft wing. The purpose of the challenge is to further develop variable amplitude models for virtual testing and digital twin applications [9]. Eq. (27) and the FSI approach was used in our blind prediction (submission 1) and gave the best prediction compared to other state-of-the-art methods [91]. Details of submission 1 is given in the supplementary material.

6. Conclusions

A new, dimensionally correct FCGR equation (Eq. (20)) for ductile engineering materials is found that is based on the original crack driving force in brittle materials and accounts for the presence of plasticity in metals. Experimental results clearly show that the parameter of similitude is proportional to the cyclic strain energy release rate and inversely proportional to the maximum stress intensity factor. Hence, crack extension during cyclic loading is driven by the range of strain energy instead of the range of stress as advocated by the Paris law. The new parameter of similitude simplifies to $\Delta K/E$ for $R = 0$ and to an equation that is proportional to ΔK_{eff} for $R > 0$.

The new approach gives a physical explanation for the stress ratio effect, which is usually attributed to crack closure in literature, and it accounts for crack growth retardation under variable amplitude loading. The method has been successfully applied to VA crack growth in 7075-T7351 material, where the spectra are representative of different fatigue dominated aircraft locations. As such, it allows for accurate predictions of variable amplitude fatigue (crack growth) life in engineering structures and components.

It is concluded that the novel approach presented is an essential step in deriving *ab initio* the fatigue crack growth rate equation and provides an attractive contribution to the development of future digital twin technology and advanced crack growth resistant materials.

CRediT authorship contribution statement

Emiel Amsterdam: Conceptualization, Formal analysis, Funding acquisition, Investigation, Methodology, Project administration, Resources, Supervision, Validation, Visualization, Writing - original draft. **Jan Willem E. Wiegman:** Data curation, Software. **Marco Nawijn:** Data curation, Software. **Jeff Th.M . De Hosson:** Writing – review & editing.

Declaration of Competing Interest

The authors declare that they have no known competing financial interests or personal relationships that could have appeared to influence the work reported in this paper.

Data availability

Data will be made available on request.

Acknowledgements

The authors would like to thank Marcel Bos for his comments on the manuscript. This work was part of a public-private partnership project called “Prediction of fatigue in engineering alloys” (PROF). Financial contributions from the Netherlands Ministry of Economic

Affairs and Climate Policy, through TKI-HTSM and the Materials Transition Programme, the Netherlands Ministry of Defence, GKN Fokker, Embraer, Airbus, Wärtsilä and Lloyd's Register are gratefully acknowledged. Scientific discussions with Tim Janssen (GKN Fokker), Giorgia Aleixo, Marcelo de Barros (Embraer), Derk Daverschot (Airbus), Jiajun Wang, Aarif Zaheer (Wärtsilä), Weihong He, Li Xu (Lloyd's Register), Jesse van Kuijk and René Alderliesten (TU Delft) are highly acknowledged.

Appendix A. Supplementary data

Supplementary data to this article can be found online at https://doi.org/10.1016/j.engfracmech.2023.109292.

References

[1] Griffith AA. The Phenomena of Rupture and Flow in Solids. Philos Trans Ser A 1920;221:163–98.
[2] Irwin GR. Analysis of Stresses and Strains near the End of a Crack Traversing a Plate. J Appl Mech 1957;24:361–4.
[3] Paris PC, Erdogan F. A critical analysis of crack propagation laws. J Basic Engng 1963:528–33.
[4] Suresh S. Fatigue of materials. 2nd ed. Cambridge; New York: Cambridge University Press; 1998.
[5] Martin DE, Sinclair GM. Crack propagation under repeated loading. Proceedings of the Third U.S. Congress of Applied Mechanics, 1958.
[6] Frost NE, Greenan AF. Cyclic stress required to propagate edge cracks in eight materials. J Mech Engng Sci 1964;6(3):203–10.
[7] Pearson S. Fatigue crack propagation in metals. Nature 1966;211(5053):1077–8.
[8] Elber W. The Significance of Fatigue Crack Closure. ASTM STP486 Damage Tolerance in Aircraft Structures 1971:230–41.
[9] Wong AK. Blueprint TITANS: A Roadmap towards the Virtual Fatigue Test through a Collaborative International Effort. Proceedings of the 35th ICAF Conference and 29th ICAF Symposium, Nagoya, Japan: 2017, p. 1–9.
[10] Vormwald M. Multi-challenge aspects in fatigue due to the combined occurrence of multiaxiality, variable amplitude loading, and size effects. Frattura Ed Integrità Strutturale 2015;9:253–61. https://doi.org/10.3221/IGF-ESIS.33.31.
[11] Kahn SU, Alderliesten RC, Schijve J, Benedictus R. On the fatigue crack growth prediction under variable amplitude loading. Comput Exp Anal Damaged Mater 2007:77–105.
[12] Paris P. Service load fatigue damage - a historical perspective. Int J Fatigue 1999;21:35–46. https://doi.org/10.1016/S0142-1123(99)00054-7.
[13] James MN. Some unresolved issues with fatigue crack closure–measurement, mechanism and interpretation problems. Proceedings of the Ninth Int. Conf. on Fracture, Sydney, Australia: Pergamon Press; 1997, p. 2403–14.
[14] Paris PC, Gomez MP, Anderson WE. A rational analytic theory of fatigue. The Trend Eng 1961;13:9–14.
[15] Amsterdam E, Grooteman F. The influence of stress state on the exponent in the power law equation of fatigue crack growth. Int J Fatigue 2016;82:572–8. https://doi.org/10.1016/j.ijfatigue.2015.09.013.
[16] Schijve J. Fatigue crack closure, observations and technical significance. Delft University of Technology; 1986.
[17] Walker K. The effect of stress ratio during crack propagation and fatigue for 2024-T3 and 7075-T6 aluminum. Effects of environment and complex load history on fatigue life, ASTM STP 462; 1970.
[18] James MN, Wenfong L. Fatigue crack growth in austempered ductile and grey cast irons—stress ratio effects in air and mine water. Mater Sci Engng A 1999;265: 129–39. https://doi.org/10.1016/S0921-5093(98)01140-X.
[19] Mercer C, Soboyejo ABO, Soboyejo WO. Micromechanisms of fatigue crack growth in a single crystal Inconel 718 nickel-based superalloy. Acta Mater 1999;47: 2727–40. https://doi.org/10.1016/S1359-6454(99)00123-8.
[20] Noroozi A, Glinka G, Lambert S. A two parameter driving force for fatigue crack growth analysis. Int J Fatigue 2005;27:1277–96. https://doi.org/10.1016/j.ijfatigue.2005.07.002.
[21] Noroozi A, Glinka G, Lambert S. A study of the stress ratio effects on fatigue crack growth using the unified two-parameter fatigue crack growth driving force. Int J Fatigue 2007;29:1616–33. https://doi.org/10.1016/j.ijfatigue.2006.12.008.
[22] Sousa RA, Castro JTP, Lopes AAO, Martha LF. On improved crack tip plastic zone estimates based on T-stress and on complete stress fields. Fatigue Fract Engng Mater Struct 2013;36:25–38. https://doi.org/10.1111/j.1460-2695.2012.01684.x.
[23] James MN, Christopher CJ, Lu Y, Patterson EA. Local crack plasticity and its influences on the global elastic stress field. Int J Fatigue 2013;46:4–15. https://doi.org/10.1016/j.ijfatigue.2012.04.015.
[24] Vasco-Olmo JM, James MN, Christopher CJ, Patterson EA, Díaz FA. Assessment of crack tip plastic zone size and shape and its influence on crack tip shielding. Fatigue Fract Eng Mater Struct 2016;39:969–81. https://doi.org/10.1111/ffe.12436.
[25] Lopez-Crespo P, Camas D, Antunes FV, Yates JR. A study of the evolution of crack tip plasticity along a crack front. Theor Appl Fract Mech 2018;98:59–66. https://doi.org/10.1016/j.tafmec.2018.09.012.
[26] Lin B, Alshammrei S, Wigger T, Tong J. Characterisation of fatigue crack tip field in the presence of significant plasticity. Theor Appl Fract Mech 2019;103: 102298. https://doi.org/10.1016/j.tafmec.2019.102298.
[27] Dugdale DS. Yielding of steel sheets containing slits. J Mech Phys Solids 1960;8:100–4. https://doi.org/10.1016/0022-5096(60)90013-2.
[28] Barsom JM. The dependence of fatigue crack propagation on strain energy release rate and crack opening displacement. In: Rosenfeld MS, editor. Damage Tolerance in Aircraft Structures. 100 Barr Harbor Drive, PO Box C700, West Conshohocken, PA 19428-2959: ASTM International; 1971. 1–1-15.
[29] Donahue RJ, Clark HM, Atanmo P, Kumble R, McEvily AJ. Crack opening displacement and the rate of fatigue crack growth. Int J Fract Mech 1972;8(2):209–19.
[30] Liaw PK, Lea TR, Logsdon WA. Near-threshold fatigue crack growth behavior in metals. Acta Metall 1983;31:1581–7. https://doi.org/10.1016/0001-6160(83)90155-4.
[31] Hertzberg RW. On the calculation of closure-free fatigue crack propagation data in monolithic metal alloys. Mater Sci Eng A 1995;190:25–32. https://doi.org/10.1016/0921-5093(94)09610-9.
[32] Zerbst U, Vormwald M, Pippan R, Gänser H-P, Sarrazin-Baudoux C, Madia M. About the fatigue crack propagation threshold of metals as a design criterion – A review. Eng Fract Mech 2016;153:190–243. https://doi.org/10.1016/j.engfracmech.2015.12.002.
[33] Lados DA, Paris PC. Parameters and key trends affecting fatigue crack growth. Mater Sci Eng A 2007;468–470:70–3. https://doi.org/10.1016/j.msea.2006.08.127.
[34] Paris PC, Lados D, Tada H. Reflections on identifying the real ΔKeffective in the threshold region and beyond. Eng Fract Mech 2008;75:299–305. https://doi.org/10.1016/j.engfracmech.2006.12.029.
[35] Bates RC, Clark WG. Fractography and fracture mechanics. Trans Am Soc Met 1969;62:380–9.
[36] Hahn GT, Rosenfield AR, Sarrate M. Elastic-plastic fracture mechanics. Ohio: Air Force Materials Laboratory; 1970.
[37] Ohta A, Suzuki N, Mawari T. Effect of Young's modulus on basic crack propagation properties near the fatigue threshold. Int J Fatigue 1992;14:224–6. https://doi.org/10.1016/0142-1123(92)90004-V.
[38] Wilkins D, Eisenmann J, Camin R, Margolis W, Benson R. Characterizing Delamination Growth in Graphite-Epoxy. In: Reifsnider K, editor. Damage in Composite Materials: Basic Mechanisms, Accumulation, Tolerance, and Characterization, 100 Barr Harbor Drive, PO Box C700, West Conshohocken, PA 19428-2959: ASTM International; 1982, p. 168-168–16. https://doi.org/10.1520/STP34326S.

[39] Armanios EA, Bucinell RB, Wilson DW, Asp LE, Sjögren A, Greenhalgh ES. Delamination growth and thresholds in a carbon/epoxy composite under fatigue loading. J Compos Technol Res 2001;23(2):55.
[40] Rans C, Alderliesten R, Benedictus R. Misinterpreting the results: how similitude can improve our understanding of fatigue delamination growth. Compos Sci Technol 2011;71:230–8. https://doi.org/10.1016/j.compscitech.2010.11.010.
[41] Jones R, Kinloch AJ, Hu W. Cyclic-fatigue crack growth in composite and adhesively-bonded structures: the FAA slow crack growth approach to certification and the problem of similitude. Int J Fatigue 2016;88:10–8. https://doi.org/10.1016/j.ijfatigue.2016.03.008.
[42] Alderliesten RC, Brunner AJ, Pascoe JA. Cyclic fatigue fracture of composites: what has testing revealed about the physics of the processes so far? Eng Fract Mech 2018;203:186–96. https://doi.org/10.1016/j.engfracmech.2018.06.023.
[43] Chow CL, Woo CW, Chung KT. Fatigue crack propagation in mild steel. Eng Fract Mech 1986;24:233–41. https://doi.org/10.1016/0013-7944(86)90054-8.
[44] Chow CL, Woo CW. A unified formulation of fatigue crack propagation in aluminum alloys and PMMA. Eng Fract Mech 1985;21:589–608. https://doi.org/10.1016/S0013-7944(85)80052-7.
[45] Chow CL, Lu TJ. A unified approach to fatigue crack propagation in metals and polymers. J Mater Sci Lett 1990;9:1427–30. https://doi.org/10.1007/BF00721605.
[46] Chow CL, Lu TJ. Cyclic J-integral in relation to fatigue crack initiation and propagation. Engng Fract Mech 1991;39:1–20. https://doi.org/10.1016/0013-7944(91)90018-V.
[47] Dowling N, Begley J. Fatigue Crack Growth During Gross Plasticity and the J-Integral. In: Rice J, Paris P, editors. Mechanics of Crack Growth, 100 Barr Harbor Drive, PO Box C700, West Conshohocken, PA 19428-2959: ASTM International; 1976, p. 82-82–22. https://doi.org/10.1520/STP33940S.
[48] Mowbray D. Derivation of a Low-Cycle Fatigue Relationship Employing the J-Integral Approach to Crack Growth. In: Swedlow J, Williams M, editors. Cracks and Fracture, 100 Barr Harbor Drive, PO Box C700, West Conshohocken, PA 19428-2959: ASTM International; 1976, p. 33-33–14. https://doi.org/10.1520/STP28636S.
[49] El Haddad MH, Smith KN, Topper TH. Fatigue crack propagation of shorts cracks. J Engng Mater Technol 1979;101:42–6.
[50] El Haddad MH, Dowling NE, Topper TH, Smith KN. J integral applications for short fatigue cracks at notches. Int J Fract 1980;16:15–30. https://doi.org/10.1007/BF00042383.
[51] El Haddad M, Mukherjee B. Elastic-Plastic Fracture Mechanics Analysis of Fatigue Crack Growth. In: Shih C, Gudas J, editors. Elastic-Plastic Fracture: Second Symposium, Volume II—Fracture Resistance Curves and Engineering Applications, 100 Barr Harbor Drive, PO Box C700, West Conshohocken, PA 19428-2959: ASTM International; 1983, p. II-689-II-689–19. https://doi.org/10.1520/STP36793S.
[52] Tanaka K. The cyclic J-integral as a criterion for fatigue crack growth. Int J Fract 1983;22:91–104. https://doi.org/10.1007/BF00942715.
[53] Banks-Sills L, Volpert Y. Application of the cyclic to fatigue crack propagation of Al 2024–T351. Engng Fract Mech 1991;40:355–70. https://doi.org/10.1016/0013-7944(91)90270-B.
[54] McClung RC, Chell GG, Lee Y-D, Russell DA, Orient GE. Development of a practical methodology for elastic-plastic and fully plastic fatigue crack growth. Alabama: NASA; 1999.
[55] Vormwald M. Fatigue crack propagation under large cyclic plastic strain conditions. Procedia Mater Sci 2014;3:301–6. https://doi.org/10.1016/j.mspro.2014.06.052.
[56] Barenblatt GI, Botvina LR. Incomplete self-similarity of fatigue in the linear range of crack growth. Fatigue Fract Engng Mater Struct 1980;3(3):193–202.
[57] Chan KS. Scaling laws for fatigue crack. MTA 1993;24:2473–86. https://doi.org/10.1007/BF02646526.
[58] Ritchie RO. Incomplete self-similarity and fatigue-crack growth. Int J Fract 2005;132:197–203. https://doi.org/10.1007/s10704-005-2266-y.
[59] Barenblatt GI. In: Advances in Fracture Research. Dordrecht: Springer Netherlands; 2006. p. 19–35.
[60] Amsterdam E, Wiegman JWE, Nawijn M, De Hosson JTM. The effect of crack length and maximum stress on the fatigue crack growth rates of engineering alloys. Int J Fatigue 2022;161:106919. https://doi.org/10.1016/j.ijfatigue.2022.106919.
[61] J. R. Davis & Associates, ASM International, editors. Aluminum and aluminum alloys. Materials Park, OH: ASM International; 1993.
[62] ASTM: E647-15. Test Method for Measurement of Fatigue Crack Growth Rates. West Conshohocken, PA: ASTM International; 2015. https://doi.org/10.1520/E0647-15E01.
[63] Amsterdam E. Effect of Crack Length and Reference Stress on Variable Amplitude Fatigue Crack Growth Rate. In: Niepokolczycki A, Komorowski J, editors. ICAF 2019 – Structural Integrity in the Age of Additive Manufacturing. Cham: Springer International Publishing; 2020. p. 539–50. https://doi.org/10.1007/978-3-030-21503-3_43.
[64] White PD, Barter SA, Medhekar N. Comparison of fatigue crack growth stress ratio effects under simple variable amplitude loading using fractographic and strain measurements. Int J Fatigue 2018;112:240–52. https://doi.org/10.1016/j.ijfatigue.2018.01.035.
[65] Vasco-Olmo JM, Díaz FA, James MN, Yang B. Crack tip plastic zone evolution during an overload cycle and the contribution of plasticity-induced shielding to crack growth rate changes. Fatigue Fract Eng Mater Struct 2018. https://doi.org/10.1111/ffe.12840.
[66] Radhakrishnan VM. Quantifying the parameters in fatigue crack propagation. Eng Fract Mech 1980;13:129–41. https://doi.org/10.1016/0013-7944(80)90048-X.
[67] Yoder GR, Cooley LA, Crooker TW. Quantitative analysis of microstructural effects on fatigue crack growth in widmanstätten Ti-6A1-4V and Ti-8Al-1Mo-1V. Eng Fract Mech 1979;11:805–16. https://doi.org/10.1016/0013-7944(79)90138-3.
[68] Wanhill R, Galatolo R, Looije C. Fractographic and microstructural analysis of fatigue crack growth in a Ti-6Al-4V fan disc forging. Int J Fatigue 1989;11:407–16. https://doi.org/10.1016/0142-1123(89)90179-5.
[69] Wang H. A study on the change of fatigue fracture mode in two titanium alloys. Fatigue Fract Eng Mater Struct 1998;21:1077–87. https://doi.org/10.1046/j.1460-2695.1998.00095.x.
[70] Mills WJ, Brown CM. Fatigue fracture surface morphology for alloy 718. Superalloys 718, 625, 706 and various derivatives, TMS; 2001.
[71] Kunz J, Nedbal I, Siegl J, Pártl O. Detailed study of stage II of fatigue crack propagation. In: Workshop 93. Prague: Czech Technical University; 1993. p. 193–4.
[72] Yoder GR, Cooley LA, Crooker TW. On microstructural control of near-threshold fatigue crack growth in 7000-series aluminum alloys. Scr Metall 1982;16:1021–5. https://doi.org/10.1016/0036-9748(82)90448-3.
[73] Wanhill RJH. Low stress intensity fatigue crack growth in 2024–T3 and T351. Engng Fract Mech 1988;30:233–60. https://doi.org/10.1016/0013-7944(88)90227-5.
[74] Forsyth PJE. A two stage process of fatigue crack growth. Crack Propagation: Proceedings of Cranfield Symposium, Cranfield: Her Majesty's Stationery Office; 1961, p. 76–94.
[75] Forsyth PJE. Fatigue damage and crack growth in aluminium alloys. Acta Metall 1963;11:703–15. https://doi.org/10.1016/0001-6160(63)90008-7.
[76] Stofanak RJ, Hertzberg RW, Leupp J, Jaccard R. On the cyclic behavior of cast and extruded aluminum alloys. Part B: Fractogr Eng Fract Mech 1983;17(6):541–54.
[77] James LA, Mills WJ. Effect of heat-treatment and heat-to-heat variations in the fatigue-crack growth response of alloy 718. Eng Fract Mech 1985;22:797–817. https://doi.org/10.1016/0013-7944(85)90109-2.
[78] Mercer C, Soboyejo ABO, Soboyejo WO. Micromechanisms of fatigue crack growth in a forged Inconel 718 nickel-based superalloy. Mater Sci Eng A 1999;270:308–22. https://doi.org/10.1016/S0921-5093(99)00214-2.
[79] Tanaka K, Masuda C, Nishijima S. The generalized relationship between the parameters C and m of Paris' law for fatigue crack growth. Scr Metall 1981;15:259–64. https://doi.org/10.1016/0036-9748(81)90340-9.
[80] Fleck NA, Kang KJ, Ashby MF. The cyclic properties of engineering materials. Acta Metall Mater 1994;42:365–81. https://doi.org/10.1016/0956-7151(94)90493-6.
[81] Callister WD. Materials science and engineering: an introduction. 5th ed. New York: Wiley; 2000.
[82] Broek D, Schijve J. The influence of the mean stress on the propagation of fatigue cracks in aluminum alloy sheet. Netherlands Aerospace Centre (NLR); 1963.
[83] Schijve J. Analysis of the fatigue phenomenon in aluminium alloys. Netherlands Aerospace Centre (NLR); 1964.

[84] Jones R, Singh Raman RK, McMillan AJ. Crack growth: Does microstructure play a role? Eng Fract Mech 2018;187:190–210. https://doi.org/10.1016/j.engfracmech.2017.11.023.
[85] Newman Jr. JC, Wu XR, Venneri SL, Li CG. Small-crack effects in high-strength aluminum alloys - A NASA/CAE cooperative program. 1994.
[86] Wheeler OE. Spectrum loading and crack growth. J Basic Eng 1972;94:181–6. https://doi.org/10.1115/1.3425362.
[87] Gallagher JP. Estimating fatigue-crack lives for aircraft: techniques: Fatigue-crack incrementation-miniblock approaches are developed to determine crack-growth lives for steady-state, variable-amplitude loadings. Exp Mech 1976;16:425–33. https://doi.org/10.1007/BF02410350.
[88] McDonald M. Guide on the effective block approach for the fatigue life assessment of metallic structures. DSTO Defence Science and Technology Organisation; 2013.
[89] Matsuishi M, Endo M. Fatigue of metals subjected to varying stress. Jukvoka, Japan: Japan Society of Mechanical Engineers; 1968.
[90] Rychlik I. A new definition of the rainflow cycle counting method. Int J Fatigue 1987;9:119–21. https://doi.org/10.1016/0142-1123(87)90054-5.
[91] Walker K, McCoy M, Ogden R, Maxfield K. Crack growth prediction challenge in wide 7075-T7351 panels, ASIP Conference (Virtual): http://meetingdata.utcdayton.com/agenda/asip/2020/proceedings/presentations/P20086.pdf; 2020.